Supporting Information for:

Structural Classification of Metal Complexes with Three-Coordinate Centres.

Timothy L. Davis,[a] Joshua L. Watts,[a] Kenneth J. Brown,*[a] Jeewantha S. Hewage,[b] Alexander R. Treleven,[b] Sergey V. Lindeman[b] and James R. Gardinier,*[b]

[a] Department of Chemistry, Winston-Salem State University, Winston- Salem, NC, USA 27110-0003. Fax: 336-750-2549; Tel: 336-750-2894; E-mail: brownkj@wssu.edu;

[b] Department of Chemistry, Marquette University, Milwaukee, WI, USA 53201-1881. Fax: 414-288-7066; Tel: 414-288-3533; E-mail: james.gardinier@marquette.edu

Table of Contents:

Experimental

General considerations. Pyrazole, NaH powder, thionyl chloride, anhydrous $CoCl_2$, 4-Bromoacetanilide, 4-formylbenzeneboronic acid, ferrocenecarboxaldehyde, 2,2'-pyridyl, and all silver salts were purchased commercially and were used as received. $Pd(PPh_3)_4$[S1] was prepared according to a literature procedure. THF was distilled under nitrogen from a deep blue sodium benzophenone ketyl solution prior to use.

Instrumentation. Midwest MicroLab, LLC, Indianapolis, Indiana 45250, performed elemental analyses for **1** while Robertson Microlit Laboratories of Ledgewood, NJ, 07852 performed analysis on **L2**, **2**·CH_2Cl_2. IR spectra were acquired on solid samples using a Thermo Scientific Nicolet iS5 IR spectrometer equipped with an iD3 Attenuated Total Reflection (ATR) accessory. ^1H (400 MHz) and ^{13}C (100.52 MHz) NMR spectra were recorded on a Varian spectrometer while NMR spectra for **L2** and **2** were recorded on a Bruker spectrometer, ^1H (300 MHz) and ^{13}C (75.47 MHz). Chemical shifts were referenced to solvent resonances at δ_H 7.26, δ_C 77.16 for $CDCl_3$; δ_H 1.94, δ_C 118.26 for CD_3CN and δ_H 2.50, δ_C 39.52 for $(CD_3)_2SO$ Melting point determinations were made on samples contained in glass capillaries using an Electrothermal 9100 apparatus or a Barnstead International 1201D unit (**L2** and **2**) and are uncorrected.

Ligand Syntheses.

4-[$CH_3C(O)NH$]$C_6H_4C_6H_4C(O)H$.

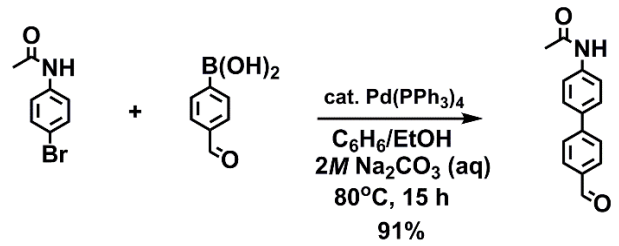

In an argon-filled drybox, a Schlenk flask was charged with 1.460 g (6.821 mmol) 4-Bromoacetanilide, 1.024 g (6.829 mmol) 4-formylbenzeneboronic acid and 0.684 g (0.673 mmol, 10 mol%) $Pd(PPh_3)_4$. After the flask was removed from the drybox and attached to a Schlenk line, two solutions that had previously been purged with argon 15 min were added sequentially via cannula; the first solution was a mixture of 10 mL absolute ethanol in 30 mL benzene and the second solution was 10 mL of 2*M* aqueous Na_2CO_3. After the magnetically-stirred biphasic mixture had been heated at 80 °C with the aid of external oil bath for 15 h, the mixture was cooled to room temperature and poured into 100 mL H_2O. A precipitate of the desired compound was formed immediately and was collected by suction filtration, was washed with 20 mL absolute ethanol, and was dried under vacuum to give 1.490 g (91 % yield) of 4-[$CH_3C(O)NH$]$C_6H_4C_6H_4C(O)H$ as an ash-coloured solid. Mp, 198-199 °C. ^1H NMR: ($CDCl_3$) 10.04 (s, 1 H, CHO), 7.93 (d, *J* = 8.2 Hz, 2 H, Ar), 7.72 (d, *J* = 8.2 Hz, 2 H, Ar), 7.64 (d, *J* = 8.7 Hz, 2 H, Ar), 7.60 (d, *J* = 8.7 Hz, 2 H, Ar), 7.50 (br s, 1 H, NH), 2.22 (s, CH_3). ^{13}C NMR: ($CDCl_3$) 192.2, 168.6, 138.6, 135.6, 135.2, 133.6, 130.6, 128.1, 127.5, 120.4, 24.9.

4-$NH_2C_6H_4C_6H_4CHpz_2$, L1

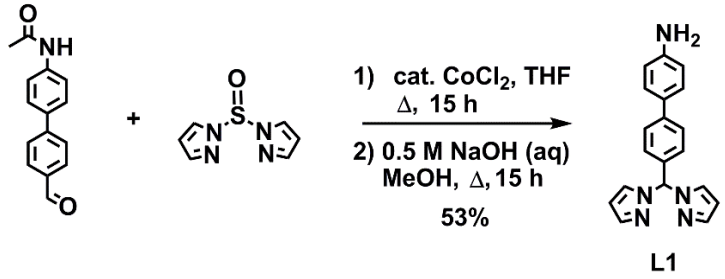

A solution of 0.427 g (6.27 mmol) 1H-pyrazole (Hpz) in 10 mL THF was added to a suspension of 0.151 g (6.29 mmol) NaH in 10 mL THF via cannula at a rate slow enough to control hydrogen evolution. The flask originally containing pyrazole was washed with an additional 5 mL of THF to ensure quantitative transfer. After the hydrogen evolution ceased, a solution of 0.23 mL (3.1 mmol) $S(O)Cl_2$ in 10 mL THF was added to the solution of Na(pz) whereupon a colourless precipitate of NaCl formed. After the suspension of $S(O)pz_2$/NaCl had been stirred 30 min, 0.027 g (0.021 mmol) $CoCl_2$ was added in one portion under an argon blanket. After the resulting blue suspension had been stirred 5 min, 0.500 g (2.07 mmol) 4-$[CH_3C(O)NH]C_6H_4C_6H_4C(O)H$ was added under an argon blanket. The suspension was heated at reflux 15 h, then solvents were removed by vacuum distillation. Next, 0.850 g (21.3 mmol) NaOH, 40 mL distilled H_2O, and 20 mL methanol were added to the solid residue and the mixture was subsequently heated at reflux 15 h. After, the mixture was cooled to room temperature, 50 mL of ethyl acetate was added. The aqueous and organic fractions were separated and the aqueous fraction was extracted with two 50 mL portions of ethyl acetate. The combined organic fractions was dried over $MgSO_4$ and solvents were removed by rotary evaporation to leave a brown oil. The brown oil was subjected to column chromatography using 1:1 hexane:ethyl acetate as the eluent. The desired compound was recovered from the third fraction (R_f = 0.42), after removing solvent by vacuum distillation, to yield 0.350 g (53 %) **L1** as colourless solid. Mp, 158 -159 ^oC. ^1H NMR: ($CDCl_3$) 7.76 (s, 1 H, CH), 7.65 (dd, *J* = 1.7, 0.4 Hz, 2 H, H_3pz), 7.55 (d, *J* = 2.3 Hz, 2 H, H_5pz), 7.52 (d, *J* = 8.5 Hz, 2 H, Ar), 7.38 (d,

J = 8.6 Hz, 2 H, Ar), 7.06 (d, *J* = 8.5 Hz, 2 H, Ar), 6.74 (d, *J* = 8.6 Hz, 2 H, Ar), 6.35 (t, *J* = 2.1 Hz, 2 H, H_4pz), 3.78 (s, 2 H, NH_2). ^{13}C NMR: ($CDCl_3$) 146.5, 142.4, 141.0, 134.0, 130.5, 129.9, 128.2, 127.5, 126.9, 115.5, 106.8, 77.9.

2-Ferrocenyl-4,5-di(2-pyridyl)imidazole, **L2.**

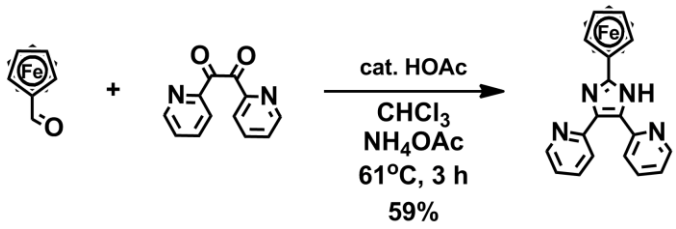

Compound **L2** was prepared following an adaptation of a literature procedure.[S2] To a 100 mL round-bottom flask under nitrogen was added 0.540 g (2.52 mmol) ferrocenecarboxaldehyde, 0.534 g (2.52 mmol) 2,2'-pyridil, 1.72 g (23.8 mmol) ammonium acetate, and 40 mL of $CHCl_3$. Glacial acetic acid (2 mL) was added, and the red mixture was heated at reflux for 3 hr. Upon cooling to room temperature, the dark red solution was neutralized with 5 mL of saturated aqueous sodium bicarbonate. The organic layer was extracted with methylene chloride (3 x 20 mL), washed with water (1 x 50 mL), and dried over sodium sulfate. After filtration of the drying agent, solvents were removed via rotary evaporation resulting in an oily brown residue. The residue was dissolved in CH_2Cl_2 and purified by column chromatography on SiO_2. The column was initially flushed with CH_2Cl_2 to remove starting materials followed by a 5% MeOH in CH_2Cl_2 solution to remove **L2**. Appropriate fractions containing **L2** (R_f in 5% MeOH/CH_2Cl_2 = 0.5) were combined and dried yielding 0.604 g (59 %) of **L2** as an orange-brown powder. Mp, 182-185 °C (Decomposed). Anal. Calcd (obs.) for $C_{23}H_{18}N_4Fe$: C, 68.00 (67.63); H, 4.47 (4.77); N, 13.79 (13.72). IR (s, ATR) ν_{NH}: 3487 cm^{-1}. ^{1}H NMR: ($CDCl_3$) 10.80 (s br, 1 H, NH), 8.68 (br, 1 H, py), 8.54 (br d, 2 H, py), 8.06 (d, *J* = 9.0 Hz, 1 H, py), 7.79 (t, *J* = 9.0, 6.0 Hz, 1 H, py), 7.66 (t, *J* = 9.0, 6.0 Hz, 1 H, py), 7.24 (br m, 1 H, py), 7.14 (br m, 1 H, py), 4.88 (d, *J* = 3 Hz, 2 H, C_5H_4), 4.35 (d, *J* = 3 Hz, 2 H, C_5H_4), 4.14 (s, 5 H, C_5H_5). ^{13}C NMR: ($CDCl_3$) 148.5, 148.4, 147.5, 136.7, 123.7, 122.1, 100.0, 93.4, 74.3, 69.6, 69.4, 69.2,

66.7. ^{1}H NMR: ($(CD_3)_2SO$) 13.23 (s, 1 H, NH), 8.86 (d, *J* = 6.0 Hz, 1 H, py), 8.53 (d, *J* = 6.0 Hz, 1H, py), 8.11 (t, *J* = 6.0, 9.0 Hz, 1 H, py), 7.89 (d, *J* = 9.0 Hz, 1 H, py), 7.78 (t, *J* = 9.0, 6.0 Hz, 1 H, py), 7.65 (d, *J* = 6.0 Hz, 2 H, py), 7.34 (t, *J* = 6.0, 6.0 Hz, 1 H, py), 5.07 (t, *J* = 3.0, 3.0 Hz, 2 H, C_5H_4), 4.35 (m br, 2 H, C_5H_4), 4.05 (s, 5 H, C_5H_5). ^{13}C NMR: ($(CD_3)_2SO$) 154.4, 148.6, 148.2, 146.8, 138.3, 136.5, 136.0, 129.1, 123.2, 122.6, 121.9, 121.8, 75.1, 69.2, 68.9, 66.7. ESI+ HRMS: m/z observed 407.0968 (**L2**+H^+), expected 407.0959.

Silver Complexes.

[Ag(L1)](BF_4), 1. A solution of 0.207 g (0.655 mmol) **L1** in 10 mL THF was added to a solution of 0.128 g (0.655 mmol) Ag(BF_4) in 10 mL THF causing immediate precipitation. After the resulting suspension had been stirred at room temperature 2 h, solvent was removed by cannula filtration. The residue was washed with two 5 mL portions Et_2O and was dried at 100 °C under vacuum 4 h to leave 0.311 g (93 %) **1** as a colourless solid. Mp, 180-181 °C (Decomposed). Anal. Calcd (obs.) for $C_{20}H_{17}N_5AgBF_4$: C, 46.01 (45.88); H, 3.28 (3.30); N, 13.40 (13.02). IR (s, ATR) ν_{NH}: 3346, 3296; ν_{BF}[S3]: 1095, 1053, 1030, 1006 cm^{-1}. ^{1}H NMR: (CD_3CN) 8.01(dd, *J* = 2.5, 0.7 Hz, 2H, pz), 7.89(s, 1 H, CHO), 7.57(d, *J* = 2.0 Hz, 2 H, pz), 7.54(d, *J* = 8.6 Hz, 2 H, Ar), 7.39(d, *J* = 8.7 Hz, 2 H, Ar), 6.71(d, *J* = 8.7 Hz, 2 H, Ar), 6.69(d, *J* = 8.6 Hz, 2 H, Ar), 6.44(dd, *J* = 2.5, 2.0 Hz, 2 H, pz), 4.33(s, NH_2). ^{19}F NMR: (CD_3CN) -151.65, -151.70. ^{13}C NMR: (CD_3CN) 149.3, 143.2, 143.0, 134.0, 133.7, 129.2, 128.7, 128.2, 126.9, 115.8, 107.4, 76.5. X-ray quality crystals of **1**·$(C_3H_6O)_{0.74}(Et_2O)_{0.62}$ were grown by layering an acetone solution of **1** with Et_2O. The crystals readily lose solvent and are slightly hygroscopic. A sample that was dried under vacuum 1 hr at room temperature and exposed to atmospheric moisture for 1 d, analysed as 1·0.25 acetone·0.75 H_2O; Anal. Calcd (obs.) for $C_{20.75}H_{20}N_5AgBF_4O$: C, 45.31 (45.02); H, 3.66 (3.47); N, 12.73 (12.91).

[Ag(L2)](SbF_6)·CH_2Cl_2, 2·CH_2Cl_2. A solution of 0.224 g (0.551 mmol) **L2** in 10 mL CH_2Cl_2 was added to a solution of 0.189 g (0.550 mmol) Ag(SbF_6) in 10 mL MeOH. The solution was stirred for 1 hr over which time an orange precipitate formed. Solvent was removed by cannula filtration, and the precipitate was

subsequently washed with methanol (2 x 5 mL). The precipitate was vacuum dried yielding 0.222 g (48 %) of **2·CH_2Cl_2** as an orange powder. Mp, 252-254 °C (Decomposed). Anal. Calcd (obs.) for $C_{24}H_{20}N_4FeAgSbF_6Cl_2$: C, 34.53 (34.50); H, 2.41 (2.36); N, 6.71 (6.83). IR (s, ATR) ν_{NH}: 3312 cm^{-1}. ^1H NMR: ((CD_3)$_2$SO) ^1H NMR: ((CD_3)$_2$SO) 13.23 (s, 1 H, NH), 8.86 (d, *J* = 3.0 Hz, 1 H, py), 8.53 (d, *J* = 3.0 Hz, 1H, py), 8.10 (t, *J* = 7.8 Hz, 1 H, py), 7.88 (d, *J* = 7.8 Hz, 1 H, py), 7.78 (t, *J* = 6.7 Hz, 1 H, py), 7.65 (d, *J* = 6.7 Hz, 2 H, py), 7.62 (d, *J* = 5.7 Hz, 2 H, py), 7.34 (t, *J* = 5.7 Hz, 1 H, py), 5.74 (s, 2H, CH_2Cl_2), 5.07 (pst, *J* = 1.8 Hz, 2 H, C_5H_4), 4.35 (br m, 2 H, C_5H_4), 4.04 (s, 5 H, C_5H_5). ESI+ HRMS: m/z observed 512.9954 (**L2**Ag^+), expected 512.9935; observed 919.0847 ((**L2**)$_2Ag^+$), expected 919.0819. X-ray quality single crystals of **2**·(CH_3OH)(CH_2Cl_2)$_{0.5}$ were obtained by layering a CH_2Cl_2 solution of **L2** with an equimolar solution of $AgSbF_6$ in CH_3OH.

Crystallography.

X-ray intensity data from a colorless prism of **[Ag(L1)](BF$_4$)**·$(C_3H_6O)_{0.74}(Et_2O)_{0.62}$, **1**·$(C_3H_6O)_{0.74}(Et_2O)_{0.62}$, and an orange block of **[Ag(L2)](SbF$_6$)**·$(CH_3OH)(CH_2Cl_2)_{0.5}$, **2**·$(CH_3OH)(CH_2Cl_2)_{0.5}$ were collected at 100.0(1) K with an Oxford Diffraction Ltd. Supernova diffractometer equipped with a 135 mm Atlas CCD detector using Cu(Ka) for **1**·$(C_3H_6O)_{0.74}(Et_2O)_{0.62}$ and Mo(Ka) radiation for **2**·$(CH_3OH)(CH_2Cl_2)_{0.5}$. Raw data frame integration and Lp corrections were performed with either CrysAlis Pro (Oxford Diffraction, Ltd.)[S4] or SAINT+ (Bruker).[S5] Final unit cell parameters were determined by least-squares refinement of 15497 and 12812 reflections of **1**·$(C_3H_6O)_{0.74}(Et_2O)_{0.62}$, and **2**·$(CH_3OH)(CH_2Cl_2)_{0.5}$, respectively, with $I > 2\sigma(I)$ for each. Analysis of the data showed negligible crystal decay during collection in each case. Direct methods structure solutions were performed with Olex2.solve[S6] while difference Fourier calculations and full-matrix least-squares refinements against F2 were performed with SHELXTL.[S7] Numerical absorption corrections based on Gaussian integration over a multifaceted crystal model were applied to the data from both experiments. All non-hydrogen atoms were refined with anisotropic displacement parameters. Hydrogen atoms were placed in geometrically idealized positions and included as riding atoms. The X-ray crystallographic parameters and further details of data collection and structure refinements are given in Table S1.

Table S1. Crystallographic Data Collection and Structure Refinement for **[Ag(L1)][BF_4]**·$(C_3H_6O)_{0.74}(Et_2O)_{0.62}$, **1**·$(C_3H_6O)_{0.74}(Et_2O)_{0.62}$, **[Ag(L2)][$SbF_6$]**·$(CH_3OH)(CH_2Cl_2)_{0.5}$, **2**·$(CH_3OH)(CH_2Cl_2)_{0.5}$.

Compound	**1**·$(C_3H_6O)_{0.74}(Et_2O)_{0.62}$	**2**·$(CH_3OH)(CH_2Cl_2)_{0.5}$
Formula	$C_{42.67}H_{44.58}Ag_2B_2F_8N_{10}O_{1.35}$	$C_{24.5}H_{23}AgClF_6FeN_4OSb$
Formula weight	1108.55	824.39
Crystal system	monoclinic	triclinic
Space group	P 2_1/n	P -1
Temperature [K]	100.0(1)	100.0(1)
a [Å]	10.35064(18)	10.4401(3)
b [Å]	16.2471(3)	11.0107(4)
c [Å]	29.6352(7)	13.8825(4)
α [°]	90.00	66.887(3)
β [°]	91.3085(18)	85.557(3)
γ [°]	90.00	67.084(3)
V [Å^3]	4982.41(17)	1346.54(8)
Z	4	2
$D_{calcd.}$ [gcm^{-3}]	1.478	2.033
λ [Å] (Cu or Mo Kα)	1.54184	0.7107
μ.[mm^{-1}]	6.942	2.416
Abs. Correction	numerical	numerical
T_min/max	0.2111/0.778	0.700/0.884
F(000)	2230	802
θ range [°]	2.98 to 73.67	3.08 to 29.17
Reflections collected	44385	24078
Independent Rflns	9900 (R_{Int}=0.0429)	6494 (R_{Int}=0.0314)
Data/restr./param.	9900/0/628	6494/0/372
Goodness-of-fit on F^2	1.056	1.032
$R1^a$ /$wR2^b$ [$I>2\sigma(I)$]	0.0602/0.1707	0.0291/0.0642
*R*1/*wR*2 (all data)	0.0683 /0.1789	0.0366/0.0685
Largest diff. peak/hole / e	1.70/-1.05	0.81/-1.04

[a] $R1 = \Sigma||F_o| - |F_c||/\Sigma|F_o|$ [b] $wR2 = [\Sigma w(|F_o| - |F_c|)^2/\Sigma w|F_o|^2]^{1/2}$.

Figure S1. Asymmetric unit of **[Ag(L1)](BF$_4$)**·$(C_3H_6O)_{0.74}(Et_2O)_{0.62}$, **1**·$(C_3H_6O)_{0.74}(Et_2O)_{0.62}$ with partial atom labelling and most hydrogen atoms removed for clarity. Thermal ellipsoids are drawn at 30% probability level.

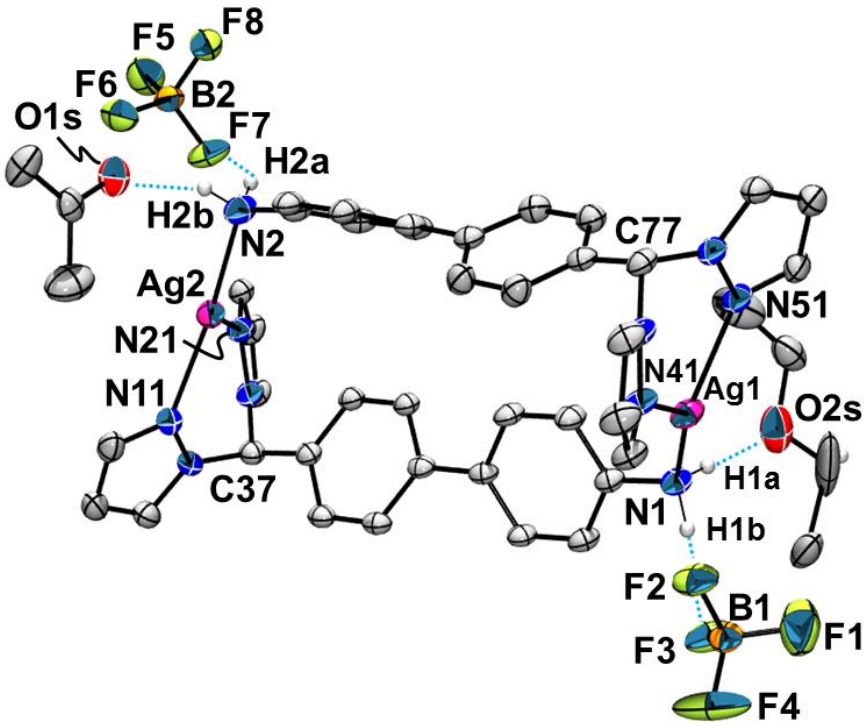

Selected bond and interatomic distances, (Å): Ag1-N1, 2.174(4); Ag1-N41, 2.266(4); Ag1-N51, 2.287(4); Ag2-N2, 2.195(5); Ag2-N11, 2.218(4); Ag2-N21, 2.390(4); N1-H1a 0.920; N1-H1b 0.920; H1a···O2s 2.05 [N1···O2s 2.971(10)]; H1b···F3 2.13 [N1···F3 3.037(6)]; N2-H2a 0.920; N2-H2b 0.920; H2a···O1s 2.16 [N2···O1s 3.034(8)]; H2b···F7 2.14 [N2···F7 2.899(7)];.
Selected bond and interatomic angles (°): N1-Ag1-N41, 139.55(18); N1-Ag1-N51, 133.26(17); N41-Ag1-N51, 86.05(16); N2-Ag2-N11, 163.98(19); N2-Ag2-N21, 111.69(18); N11-Ag2-N21, 84.31(15); N1-H1a ···O2s, 178; N1-H1a ···F3, 170; N2-H2a ···O1s, 160; N2-H2b ···F7, 139.

Figure S2. Top: Asymmetric unit of **[Ag(L2)](SbF$_6$)**·$(CH_3OH)(CH_2Cl_2)_{0.5}$, **2**·$(CH_3OH)(CH_2Cl_2)_{0.5}$ with atom labelling. Bottom: View of cyclic dication. Thermal ellipsoids are drawn at 50% probability level.

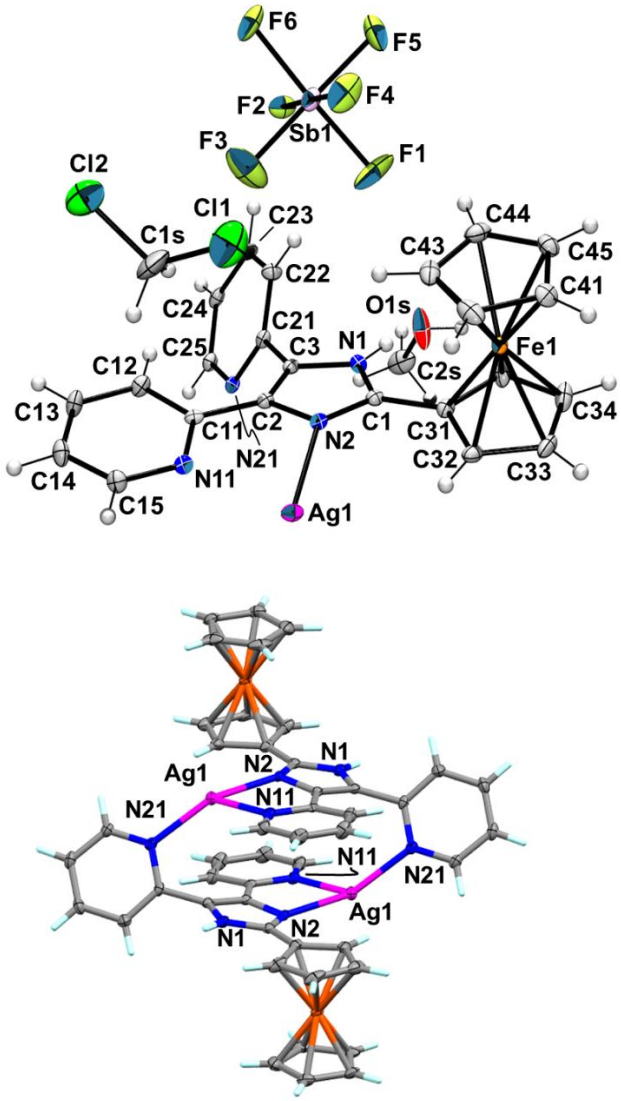

Selected bond distances, (Å): Ag1-N2, 2.238(2); Ag1-N11, 2.420(2); Ag1-N21, 2.215(2).
Selected Bond Angles (°): N2-Ag1-N11, 73.04(8); N2-Ag1-N21, 146.06(8); N11-Ag1-N21, 120.84(8).

Figure S3. Diagrams defining important distances and angles in acute (top), right (middle), and obtuse (bottom) scalene triangles (or bases of acute, normal, and obtuse triclinic pyramids) that are found in the glossary, associated spreadsheet, and described in the following text.

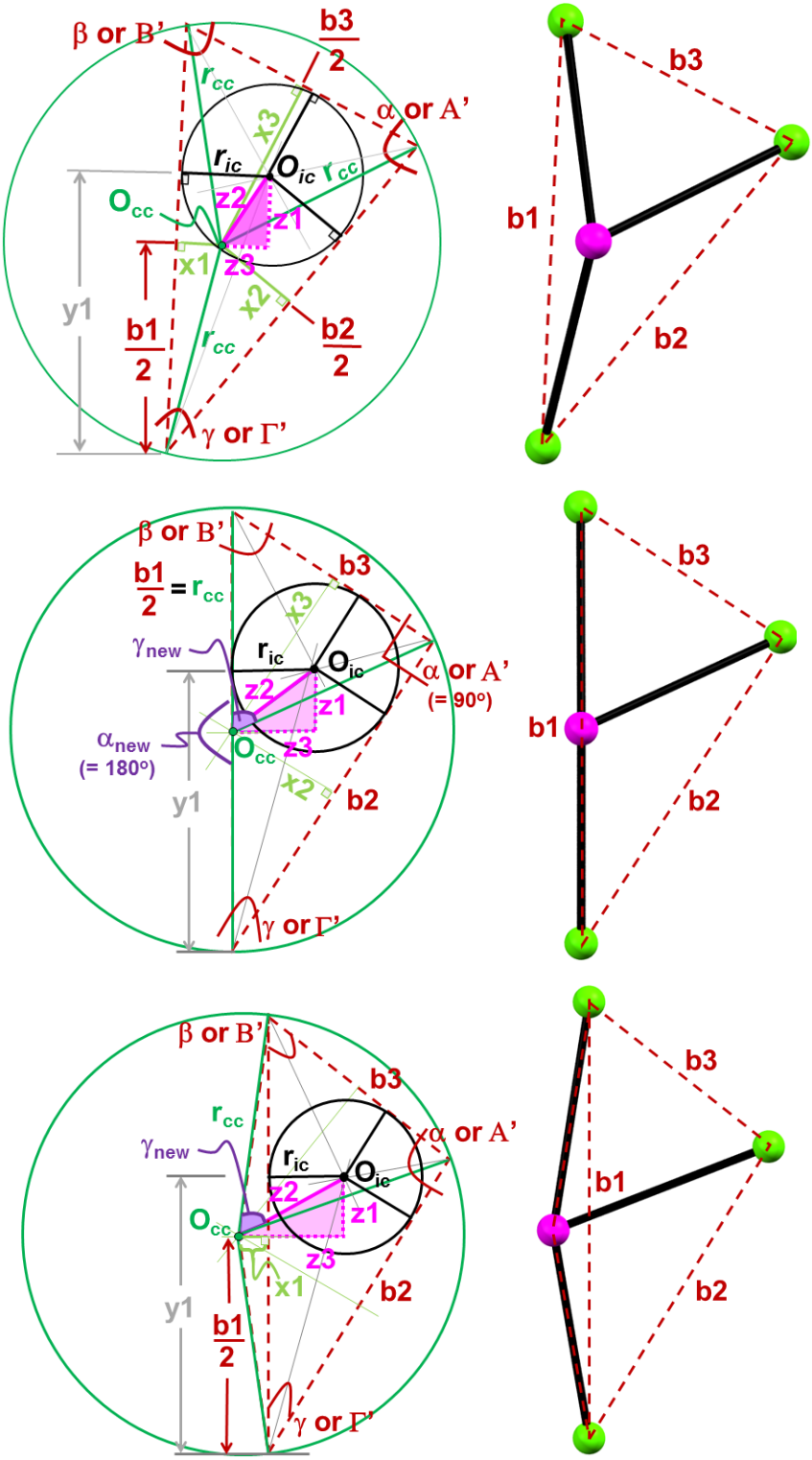

Glossary. Definition of terms for **Fig S3** and accompanying spreadsheet.

α, β, γ largest, middle, and smallest internal angles of a triangle or about the apex of a pyramid (top of side triangle).

A', B', Γ' largest, middle, and smallest internal angles of the base triangle of a pyramid

b1, b2, b3 length of base opposite of α (or A'), β (or B'), and γ (or Γ'), respectively. b1 = 2sin(α(or A')/2)

p perimeter of triangle; b1+b2+b3.

$p_{1/2}$ semiperimeter of triangle; (b1+b2+b3)/2

Ar Area of triangle. = $[(p_{1/2})(p_{1/2}\text{-}b1)(p_{1/2}\text{-}b2)(p_{1/2}\text{-}b3)]^{1/2}$

s1, s2, s3 slant height of the side triangles of a pyramid. The length of the line from the apex (bisecting α, β, or γ) to the respective base edge b1, b2, b3. s1 = cos(α/2); s2 = cos(β/2); s3 = cos(γ/2)

h height of pyramid. The length of the normal line between O_{cc} and the apex of a pyramid.

O_{cc} origin of circumcircle of triangle; defined as the point of intersection of perpendicular bisectors of b1, b2, b3.

r_{cc} radius of circumcircle of triangle. =(b1)(b2)(b3)/[(p)(b1+b2-b3)(b1+b3-b2)(b2+b3-b1)]$^{1/2}$

D_{cc} diameter of circumcircle of triangle. = 2_{rcc}

O_{ic} origin of incircle of triangle; defined as the point of intersection of the bisectors of α (or A'), β (or B'), and γ (or Γ').

r_{ic} radius of incircle of triangle. = 2Ar/p

$\alpha_{new}, \beta_{new}, \gamma_{new}$ largest, middle, and smallest angles between lines drawn from O_{cc} to each vertex of a triangle (the length of each line is r_{cc}); equivalent to twice α (or A'), β (or B'), and γ (or Γ'), respectively.

x1, x2, x3 perpendicular distance between O_{cc} and b1, b2, or b3. x1 = $[r_{cc}^2 - (b1/2)^2]^{1/2}$

y1 distance along b1 starting from the γ (or Γ') vertex to the point where the incircle touches b1 (defined by a line perpendicular to b1 and ending at O_{ic}). =[r_{ic}/tan (B'/2)]

y2 (y3) distance along b2 (b3) starting from the β or B' (α or A') vertex of to the point where the incircle touches b2 (b3) (defined by a line perpendicular to b2 (b3) and ending at O_{ic}).

z1 distance between O_{ic} and O_{cc} but parallel to b1. =Y1– ½b1

z2 distance between O_{ic} and O_{cc}. = $[z1^2 - z3^2]^{1/2}$

z3 distance between O_{ic} and O_{cc} but perpendicular to b1. = x1±r_{ic} (" - " for acute, " + " for obtuse)

$\phi 1_{incl}, \phi 2_{incl}, \phi 3_{incl}$ angle of incline between the base triangle and a side triangle of a pyramid that is hinged along b1, b2 or b3, respectively, and that is inside the pyramid.
$\phi 1_{incl}$ = $\tan^{-1}$(h/x1) = $\sin^{-1}$(h/s1) = $\cos^{-1}$(x1/s1)

Figure S4. Sampling of planar three-coordinate structures.

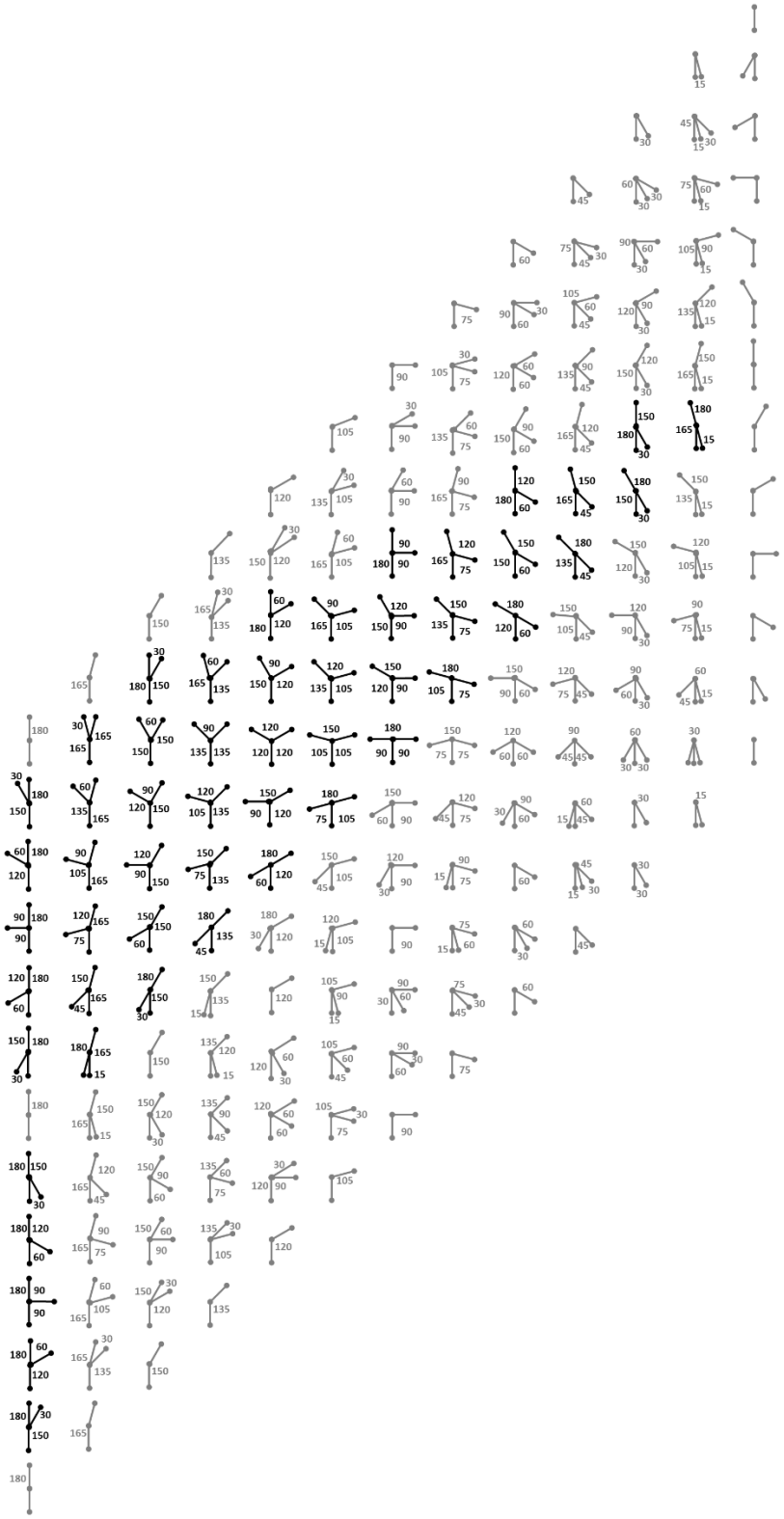

Further notes on the 3C classification system.

Y-shapes are statistically one of the more common geometries of 3C metal complexes, as can be seen in Fig S4 and in the next section describing the CSD search. Therefore, it was desirable to elaborate on the different Y-types. A trigonal plane is the most symmetric of all Y-shapes. Any other "Y's" are derived from the trigonal plane by moving the "arms" (in a plane) thereby lowering symmetry to either C_{2v} (monoclinic Y) or C_1 (triclinic Y). If one draws lines between the ligands (ends) of a trigonal plane then an equilateral triangle is formed. Similarly, lines connecting the ligands of lower symmetry shapes produce either isosceles triangles (monoclinic Y's), scalene triangles (triclinic Y's), (or even quadrilaterals if ligands are on same side, as in Arrows). Monoclinic Y's can be differentiated depending on whether α- or γ- is unique; such Y's are referred to as being either α-dominant or γ-dominant, respectively. Different γ-dominant Y's can be differentiated by comparing how small γ is relative to 0^o (Closed Y shape). Thus, between the limits of a Trigonal plane and a Closed Y, there are different levels of "constriction" that γ-dominant Y's can attain, expressed as [1-(γ/120)]*100% (or its fractional counterpart, i.e. 50% constriction = ½ constricted) as in the top of Fig S5. Similarly, between the limits of a Trigonal Plane or

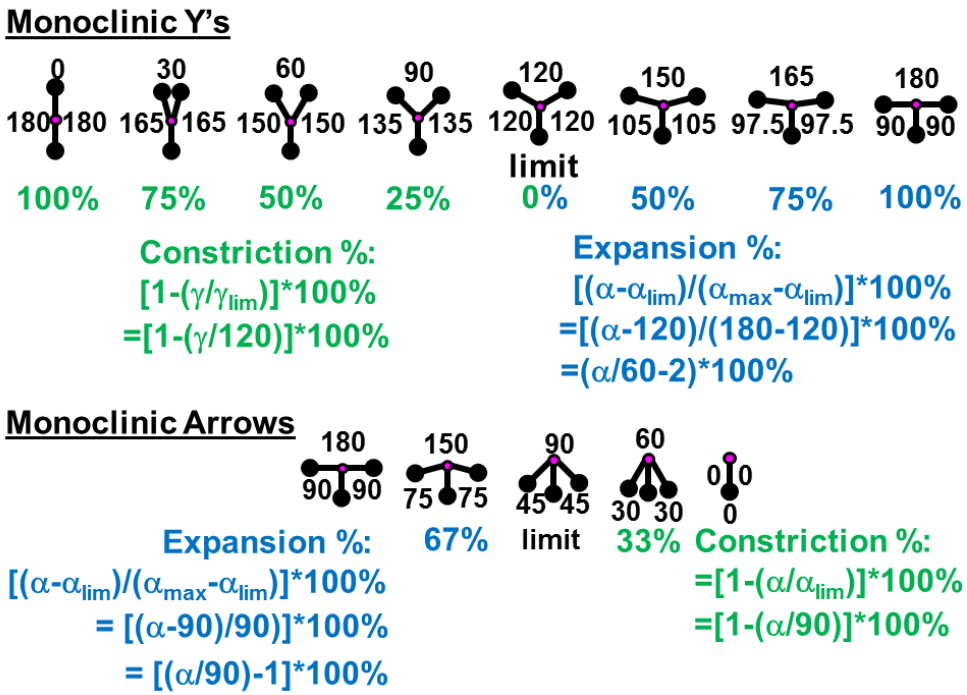

Figure S5. Expansion and Constriction in Monoclinic Y's and Arrows.

a T-shape, an α-dominant Y has varying levels of expansion, [(α/60)-2]*100%. Monoclinic Arrows ($\gamma = \beta = ½\ \alpha < 180^o$) can be differentiated in a manner similar to monoclinic Y's. Halfway between a T-shape and a Closed Arrow ($\alpha/\beta/\gamma$ = 0/0/0) is a "Normal Arrow" (90/45/45) that is used as a reference structure. Arrows between the Normal and T-shape are "α-Expanded" by [(α/90)-1]*100% (or its corresponding fractional value) whereas those between the Normal and Closed Arrow are "α-Constricted" by [1-(α/90)]*100% (or its fractional counterpart), as in the bottom of Fig S5. Triclinic Y shapes or arrows can be recognized by their own merits (such as the Orthogonal Y, 150/120/90, that is halfway between a T-shape and a Trigonal plane by rotating one arm of either 30^o) or they can be characterized according to

the "obliqueness" of the angles about the central atom. For shapes defined by α- (T-shape, Arrow, α-dominant Y's), "obliqueness" can be defined as [1-(2γ/α)]*100% (or its fractional equivalent) Fig. S6, or

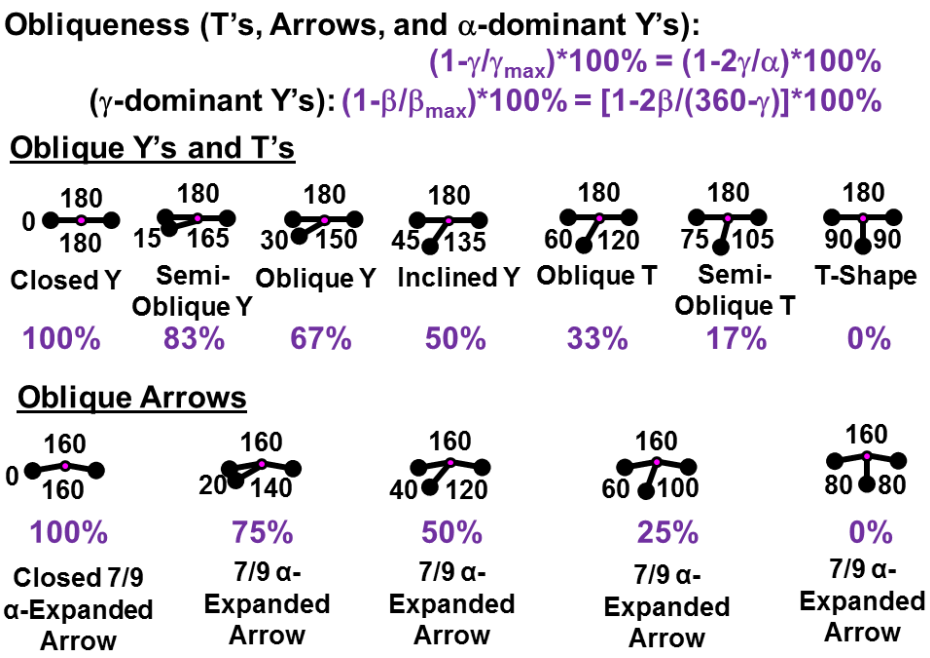

Figure S6. Obliqueness of planar 3C shapes.

how different is γ (and, hence, β) from its ideal value. We prefer this method of determining "obliqueness" over using the ratio γ/β, that is commonly used by others, since the latter actually "double counts" the distortion from ideal values. Also with the former (preferred) method it is straightforward to show that a Semi-Oblique Y (with angles 180/165/15, or 5/6 oblique) is halfway between an Oblique Y (180/150/30, 4/6 or 2/3 oblique) and a Closed Y (180/180/0, 100% or 6/6 oblique). This interrelationship would not be obvious using γ/β (1/11 vs 1/5 oblique). Next, It is noted that in γ-dominant (monoclinic) Y's, γ defines the shape, so obliqueness would need to be defined in terms of deviation of β (or α) from the ideal value of β_{max} (or α_{max}) = (360-γ)/2 or obliqueness = [1-2β/(360-γ)]*100% (or the fractional equivalent). Since triclinic Y's are defined by either α or γ and are compared to idealized structures, obliqueness does not provide any added useful information. On the other hand, since Arrows are defined precisely and only by β and γ (α =β+γ), obliqueness indeed offers useful information to describe these shapes. Therefore, in the attached spreadsheet we only include % obliqueness in the structural description of Arrows. In other cases, we leave the % obliqueness of planar triclinic "Y-" shapes for the reader to calculate manually, once a desired reference angle or structure is determined. Finally, it is useful to introduce two generic terms to describe Y-shapes irrespective of obliqueness. Extended Y's refer to those cases where α and β are greater than 120° while Compressed Y's refer to those cases where α >120° and both β and γ are between 90° and 120°. In this way, all constricted γ-dominant Y's (regardless of constriction) are Extended Y's but the converse is not necessarily true since γ-dominant Y's are defined as strictly monoclinic whereas Extended Y's cover the gamut of obliqueness. In a similar fashion, Compressed Y's include all α-dominant Y's (regardless of expansion) but, if β and γ are unequal, then Compressed Y's are not α-dominant Y's.

Pyramids. The displacement of one or more atoms of a planar three-coordinate structure out of the plane results in a pyramid. In the analysis of ideal "pyramid" structures two types of deformation were considered for simplicity. First, the motion of two arms together out of a plane while retaining two original angles was termed "folding". Figure S7 shows views of the pyramids (and ultimately the arrow)

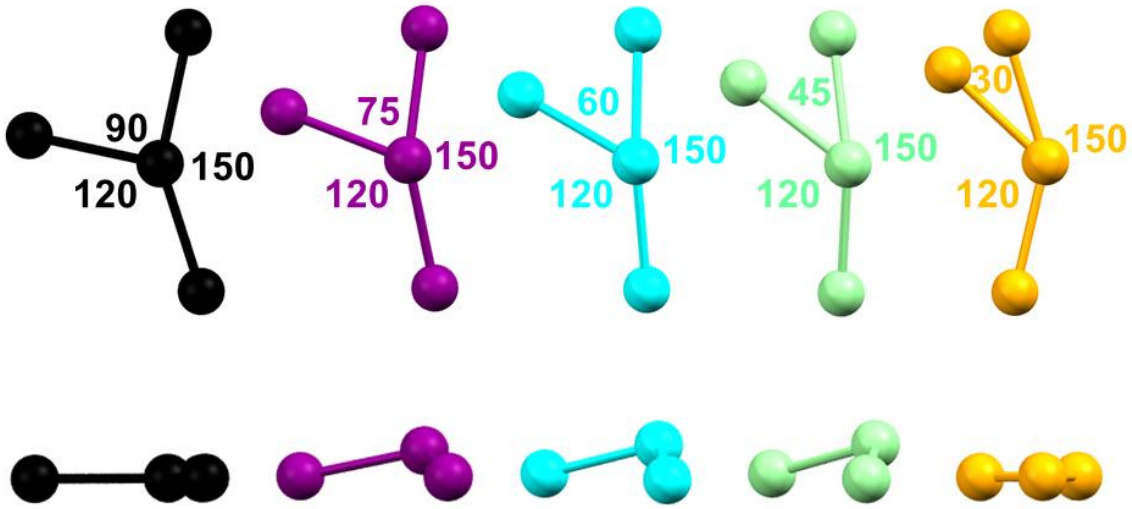

Figure S7. Folding γ between the limits of an Orthogonal Y (left, black) and a 60% oblique 2/3 α-expanded Arrow (right, orange). The top row is viewed normal to the plane of three ligands. The bottom row is a view perpendicular to the first view (parallel to two ligand atoms).

formed by folding the angle γ of an Orthogonal Y. That is, α and β are kept at 150° and 120°, respectively, while the arms containing γ are pulled together out of the plane. An acute triclinic pyramid is first formed until γ is about 52° where a normal pyramid (with an incline angle of 90°) is formed (not shown). Then, on further decreasing γ, an obtuse pyramid is formed. Finally, a planar limit (here a planar Arrow) will be reached when γ is equal to the difference between α and β, the minimum folding angle, $\gamma_{fold,min}$. Similarly β can be folded to the minimum $\beta_{fold,min}$ defined by α-γ, (Note, at a certain point the folded β will become a 'new' gamma, the $\beta_{fold,min}$ uses the original γ in the calculation and can be smaller than the original γ). Also, α can be folded until β-γ. A pyramid is recognized as a "folded planar structure" if two angles are identical to a high-symmetry, planar 3C shape as described in the previous section. Then, the % folding is calculated by comparing the folded angle to the maximum and minimum planar limits [% folding =$(\xi_{max} - \xi)/(\xi_{range} = \xi_{max} - \xi_{fold,min})]$*100% ($\xi = \alpha$, β, or γ). That is, In the Orthogonal Y example, γ has a maximum value of 90° and has a minimum of 30°, so γ can vary over a 60° range [$\gamma_{max} - \gamma_{fold,min}$]. The % γ-folding is [(90-γ)/60]*100%. If γ = 90°, the structure is planar (0% folded) whereas if γ = 60 the structure is 50% folded, etc. In a similar manner, the % α-folding of an orthogonal Y is [(150-ξ)/120]*100% ($\xi = \alpha$ for α > 120° and β =120°; $\xi = \beta$ for α =120° and 90° < β < 120°; $\xi = \gamma$ for β =90° and γ < 90°) where the conditions arise because the folded α will eventually become a new β and then a new γ on reduction. Here, the minimum α-fold angle, $\alpha_{fold,min}$, is 30° [= (β-γ) = 120° - 90°], α_{max} = 150°, and the range was 120° [$\alpha_{max} - \alpha_{fold,min}$ = 150° – 30°].

In the second type of deformation of planar 3C structures that gives pyramids, the centre atom of a 3C planar complex is moved out of the plane thereby reducing all three angles simultaneously akin to closing an umbrella. For a right pyramid, closing a pyramid is a simple reduction of the three identical

angles $\alpha = \beta = \gamma$, below 120°. The % closing of a right pyramid is $(1 - \alpha/120)*100\%$. The closing of monoclinic or triclinic planar structures is more complicated than for trigonal planar (to give right pyramids) because of the different angles about the vertex. Figure S8 shows the example of closing an Orthogonal Y. There is a series of pyramids whose O_{cc} and internal angles of base triangles are identical

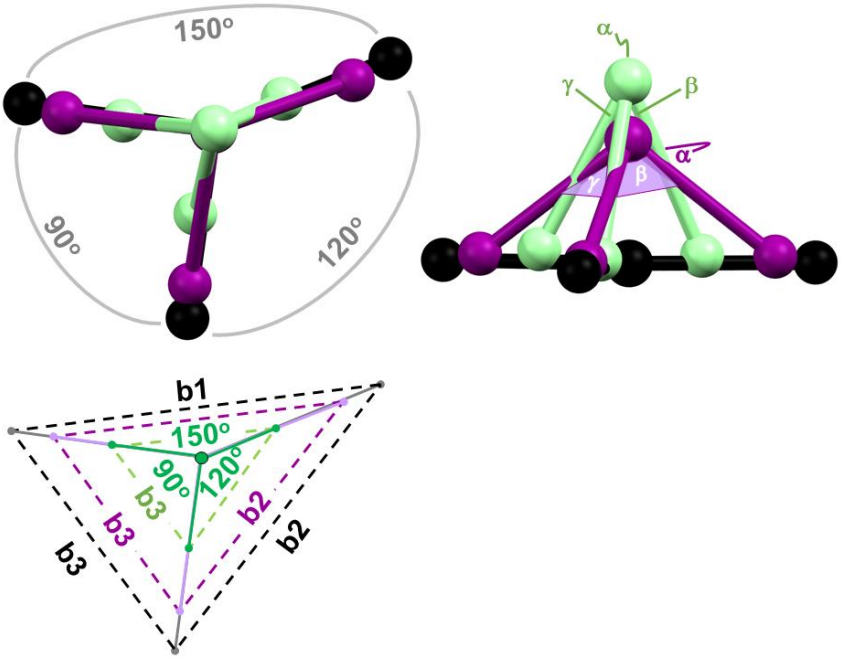

Figure S8. Overlay of a planar Orthogonal Y (black) and two pyramids (α=100°/β=87°/g=68°, purple) and (50/45/36, green) derived from 33% and 67% closing of the planar Orthogonal Y. An overlay of base triangles is also shown (lower left).

to an Orthogonal Y, but whose r_{cc} and base edges (b1, b2, b3) are smaller than those in an Orthogonal Y. The pyramids related to closing an Orthogonal Y (or any other planar structure) can be found since the ratio of base edges must be kept the same as those in Orthogonal Y upon moving the centre atom out of the plane of the three ligand atoms. Since the base edge is also related to the apex angles α, β, or γ, (= $2\sin \xi/2$) ($\xi = \alpha, \beta, \gamma$) the following relations can be used to find the apex angles in the related pyramids.

$$b3/b2 = b3'/b2'; \; b2' = b3'b2/b3; \; 2\sin \beta'/2 = (2\sin \gamma'/2)(2\sin \beta/2)/(2\sin \gamma/2);$$

$$\beta' = 2 \arcsin(\sin \gamma'/2 * \sin 60^\circ/\sin 45^\circ);$$

$$\text{Similarly, } \alpha' = 2 \arcsin(\sin \gamma'/2 * \sin 75^\circ/\sin 45^\circ);$$

The prime (') in the above relations means the apex angle of the new pyramid while the unprimed angle refers to the corresponding angles in the Orthogonal Y (or other reference planar structure). Thus, by reducing γ by an arbitrary amount (say 5°, so γ'=85°), the other angles can be calculated accordingly (β' = 111.67°; α' = 134.70°). The % closing of the pyramid can then be related to any of the three angles:

$$\% \text{ closing} = [(\alpha_{max} - \alpha')/\alpha_{max}]*100\% = [(\beta_{max} - \beta')/\beta_{max}]*100\% = [(\gamma_{max} - \gamma')/\gamma_{max}]*100\%$$

Thus, the above example with γ'=85° corresponds to a 10% closed Orthogonal Y.

Details of Cambridge Structural Database (CSD) search.

Searches of the Cambridge structural Database (Version 5.36 – 11/2014 + 1 update)[S8] were performed on $M(E)_n$ complexes where n was varied between 2 to 6, E was any nonmetal, and M was any metal. The M was constrained to have the same coordination number as the value n, thus, metal-metal bonded species were excluded. A similar set of searches was performed with the further restriction that M was Ag. Table S2 summarizes the results of these searches where it is noted that the number of entries was

Table S2. Number of ME_n centres in the CSD Database where M = any metal or Ag; E = any nonmetal, n = 2-6.

Search		M = Any metal	M = Ag
ME_2	hits	9,772	2,240
(two coordinate M)	entries	**15,364**	**3,436**
ME_3	hits	11,150	1,812
(three coordinate M)	entries	**18,001**	**2,750**
ME_4	hits	94,476	3,032
(four coordinate M)	entries	**136,596**	**4,470**
ME_5	hits	40, 084	314
(five coordinate M)	entries	**55,698**	**370**
ME_6	hits	101,108	173
(six coordinate M)	entries	**146,621**	**205**
total	hits	256,590	7,571
	entries	**372,280**	**11,231**

greater than the number of hits because there was often more than one entry per hit; some complexes were multimetallic, or the crystals had crystallographically independent groups, or both. From these results, most compounds composed of metals and nonmetals prefer higher coordination numbers; cases where n= 4-6 account for 91% of all entries. Cases where n = 3 account for 4.8 % of all entries. On the other hand, compounds of silver and nonmetals favor lower coordination numbers with n = 2-4 accounting for 94.9 % of all entries (24.5% of all are three-coordinate AgE_3).

Interestingly, an examination of the frequency of occurrence of the largest angle, α, reveals an uneven bimodal distribution of α in the general ME_3 cases (Figure S9) but a rather uniform, unimodal distribution for silver complexes (only 8 instances with $\alpha < 114^o$). The latter reflects the high frequency of the silver(I) oxidation state and the indifference of this d^{10} centre toward coordination geometry for a given coordination number. Importantly, while Fig S9 shows that the most common α angle is 127^o for ME_3 complexes and 128^o for silver and a similar analysis of β -angles reveals that 120^o to be most frequent for all, these α and β are not necessarily correlated as each spans both planar and pyramidal structures. An examination of the most common angular values (Table S3) shows these to be trigonal planar or slight distortions therefrom, but the top 15 $\alpha/\beta/\gamma$ combinations only account for 4% of all entries. Thus, scatter matrices (Figure S10) and a pivot chart (Figure S11) were constructed to better reveal angular interrelationships among all the entries.

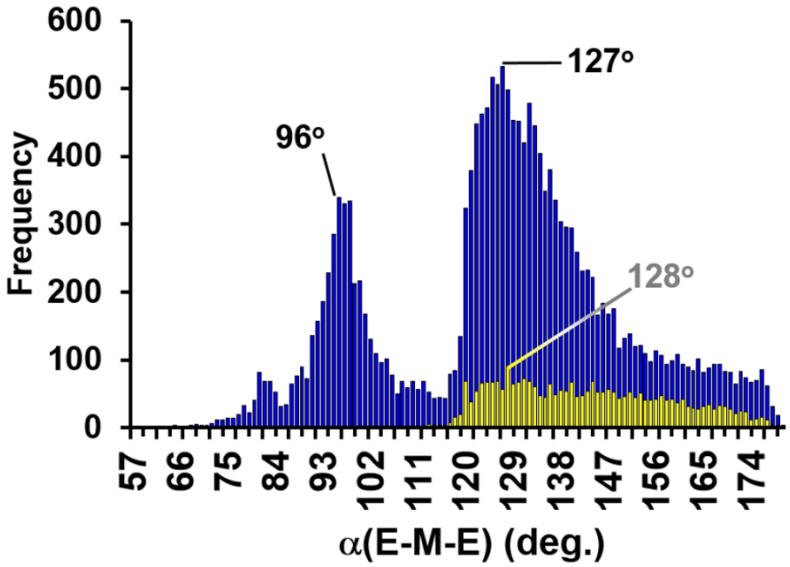

Figure S9. Histogram showing the frequency of occurrence of the largest interatomic angle (α, in deg.) in three coordinate complexes of any metal (blue, 18001 total) or of silver (yellow, 1812 total) in the CSD.

Table S3. Most common angular values (α/β/γ) for three coordinate ME_3 complexes out of 18001 entries.

Planar			Pyramidal		
Rank	**(α/β/γ)**	**Entries**	**Rank**	**(α/β/γ)**	**Entries**
1	120/120/120	156	**1**	97/96/95	28
2	121/120/119	97	**2**	92/92/92	21
3	122/120/118	65	**3**	96/96/95	20
4	122/121/117	54	**4**	96/94/93	19
5	123/120/117	50		95/94/93	
6	122/119/119	48	**5**	94/94/94	18
7	123/121/116	42		81/81/81	
	122/120/118		**6**	98/97/96	17
8	126/118/116	38	**7**	97/96/94	15
	123/122/115			95/95/94	
	120/120/119			91/91/91	
9	121/119/119	37	**8**	98/97/95	14
10	124/119/117	33		97/95/94	
	123/119/118			96/95/91	
	122/122/116		**9**	92/91/91	13
				81/81/80	

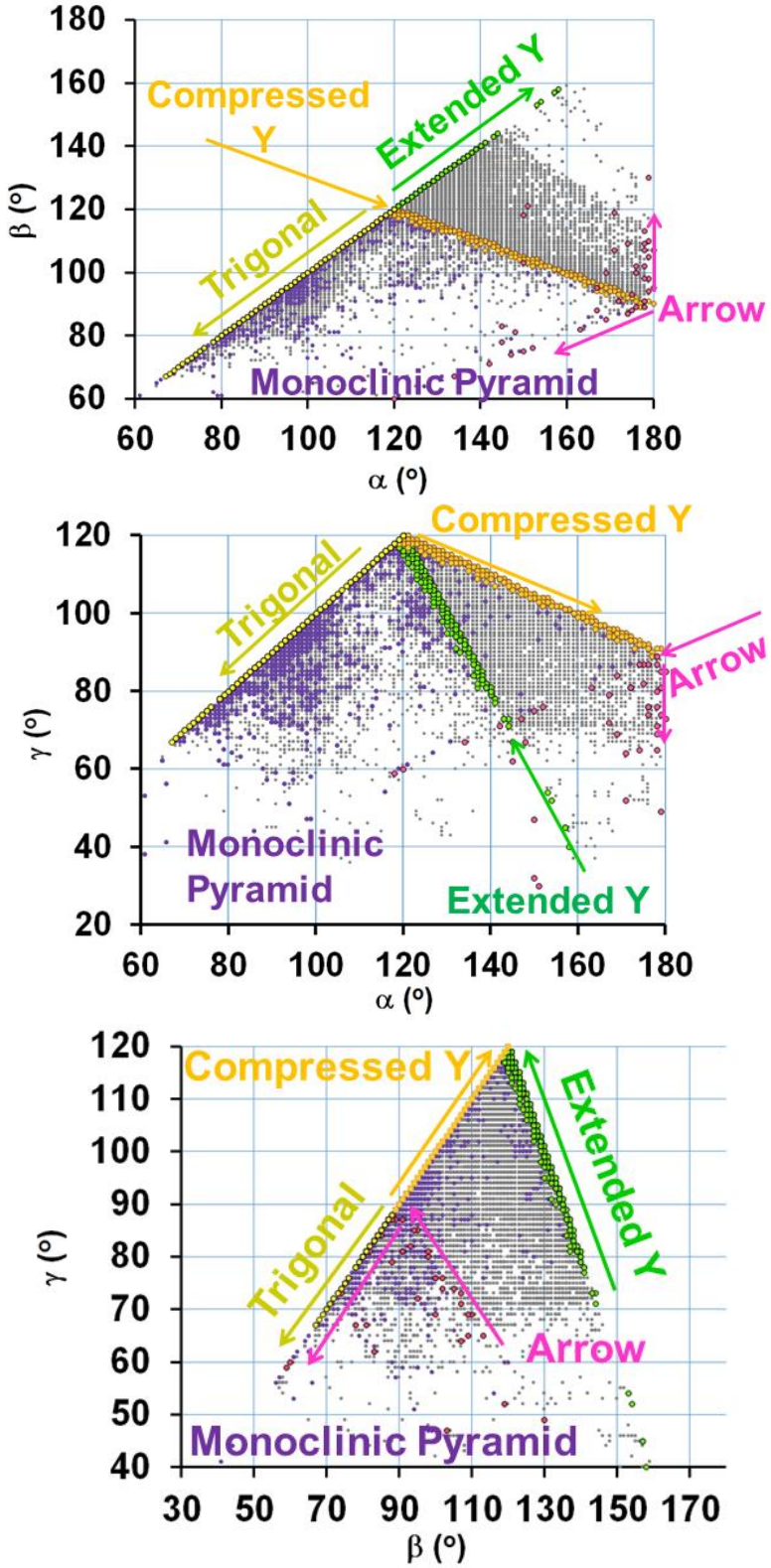

Figure S10. Scatter matrices of angular values found in CSD search of ME_3 complexes.

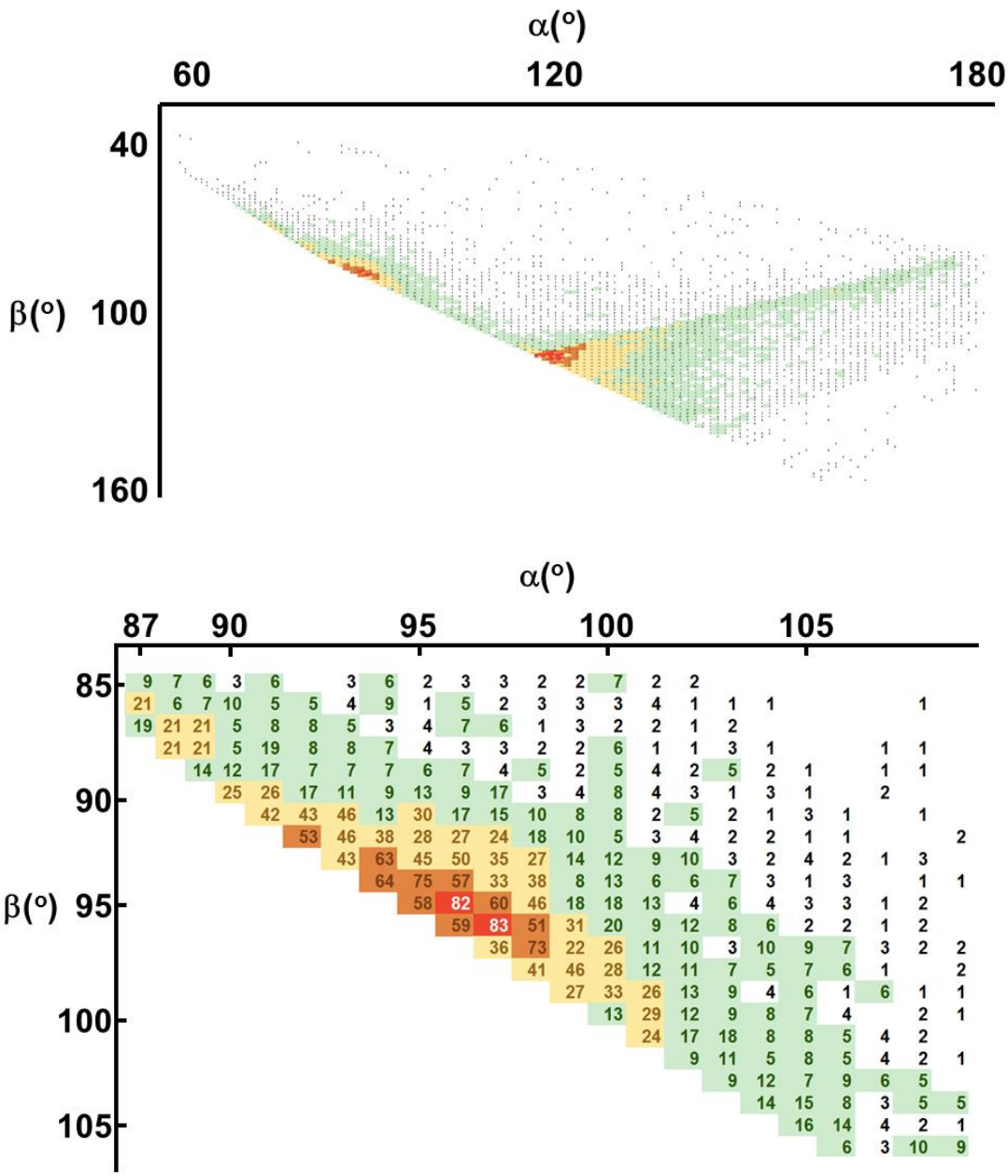

Figure S11. Pivot Chart showing frequency of α/β combinations found in the CSD search of ME_3 complexes with a blow up of the pyramidal region near $\alpha = 95^{o}/\beta = 95^{o}$. Green, 5-20 entries; Yellow, 21-50 entries; orange, 51-80 entries; red, >80 entries.

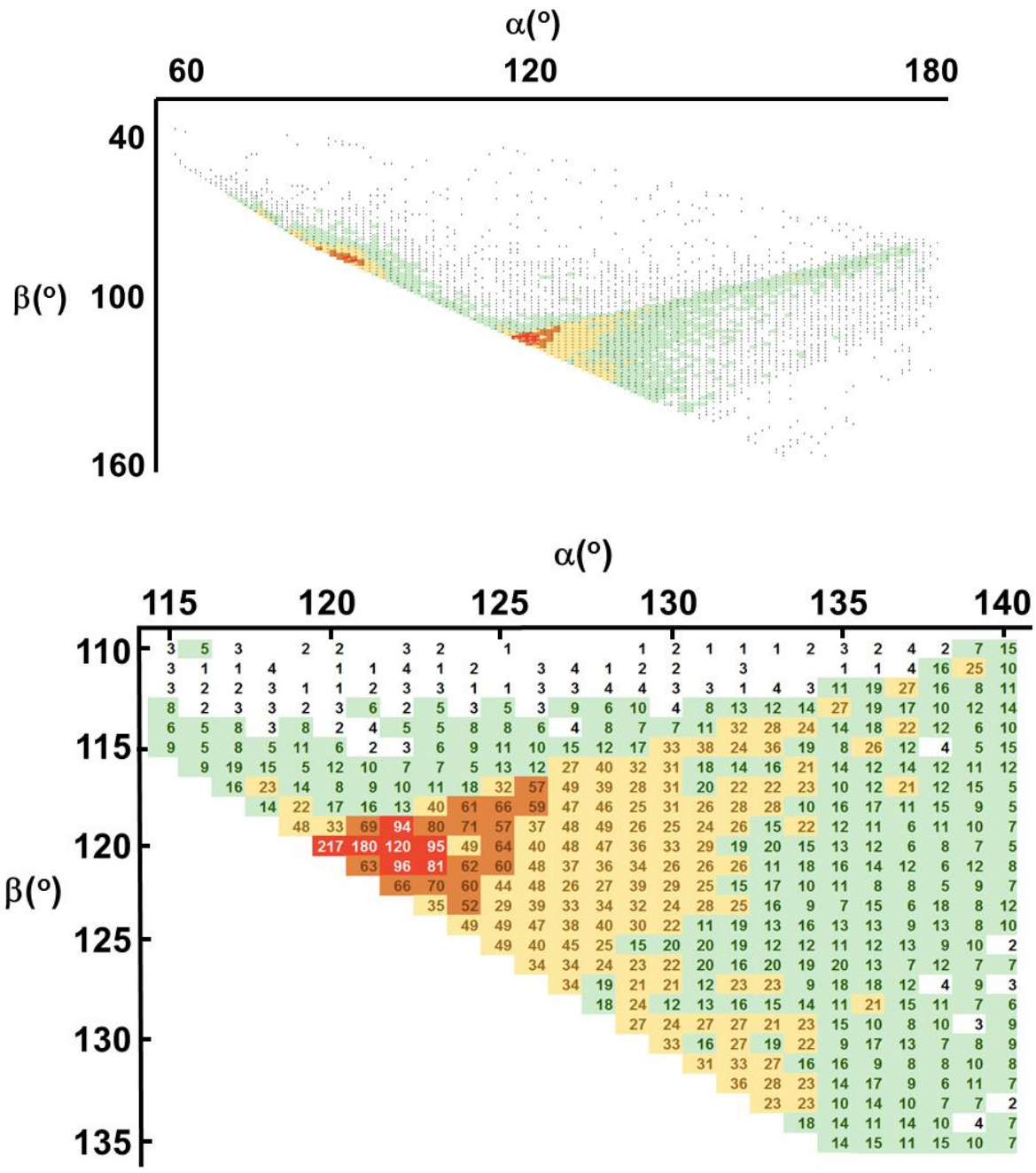

Figure S11, contd. Pivot Chart showing frequency of α/ β combinations found in the CSD search of ME_3 complexes with a blow up of the region near α = 120°/β = 120°.

Since three dimensional scatterplots are difficult to view in two dimensions, the data can be plotted as scatter matrices (α vs β, α vs γ, β vs γ, β vs α, etc.) to facilitate pattern recognition. Scatter matrices for all ME_3 entries are found in Figure S10. The data are mostly shown as grey circles with the exception of some "high-symmetry" structures which are coloured. In these plots, trigonal species ($\alpha = \beta = \gamma$) were plotted as yellow circles. These points have a slope of 1, a maximum at $\alpha = 120$, and a minimum of $\alpha = 67^o$ (CSD code: ARUGEZ). Monoclinic pyramids, those with $\Sigma\measuredangle$'s $< 354^o$ and either $\alpha = \beta$ or $\beta = \gamma$, are shown as violet dots in all plots and are rather non-uniform but random distribution with a major cluster near $\alpha = 96^o$ as might be suggested from Fig S9, the right of Table S3, or the first part of the Pivot chart in Fig. S11. Extended Y's ($\alpha = \beta > 120$; $\Sigma\measuredangle$'s $\geq 354^o$) are displayed as green circles, have a slope of 1 in the plot of β versus α, have a minimum of $\alpha = 120$ and a maximum at $\alpha = 158$ ($\Sigma\measuredangle$'s $= 356^o$, CSD code: MOMCEW). Compressed Y's ($120 > \beta = \gamma > 90$; $\Sigma\measuredangle$'s $\geq 354^o$) are shown as orange circles in the scatter matrices with a slope of -0.5 in the plot of γ versus α (+1 in the plot of γ versus β), with a minimum $\alpha = 121^o$ and a maximum of $\alpha = 179^o$ (CSD code: TEBNUK); there were two ideal T-shapes (180/90/90, CSD code: QAQJIC, WIWQOC) and six others including TEBNUK (AXUFEF, BUNFOG, CEQRIA, KAPXUW, WEYVOM) that are within 2^o in α , β, and/or γ of being an ideal T. Finally, Arrows ($\alpha = \beta + \gamma$) are shown as pink circles in the scatter matrices. The data points for monoclinic Arrow have a slope of 0.5 in the plots of γ or β versus α and a slope of +1 in the plot of γ versus β. The minimum (most constricted) Arrow has $\alpha = 118^o$ (CSD Code: KIXXUK). The data points of Oblique Arrows deviate from the previously mentioned slopes with a minimum found at 145/78/67 (CSD Code: SEYDOY).

Figure S12. ^{1}H and ^{13}C NMR spectra of **L1** in $CDCl_3$. Asterisk is for solvent resonance, arrow shows the methane carbon resonance near solvent resonance.

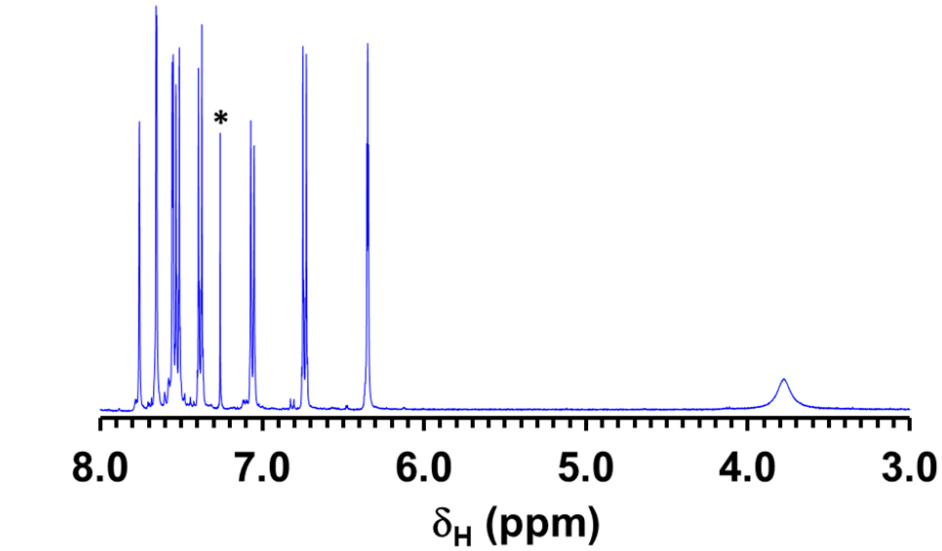

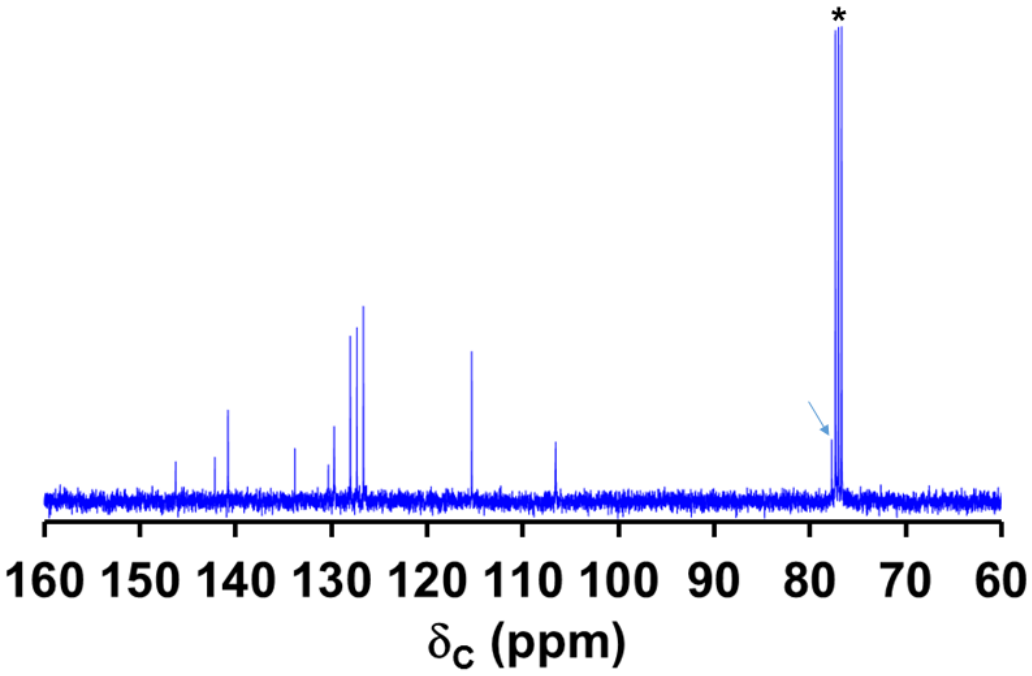

Figure S13. ^{1}H and ^{13}C NMR spectra of **L2** in dmso-d_6. Asterisk denotes signals due to solvent.

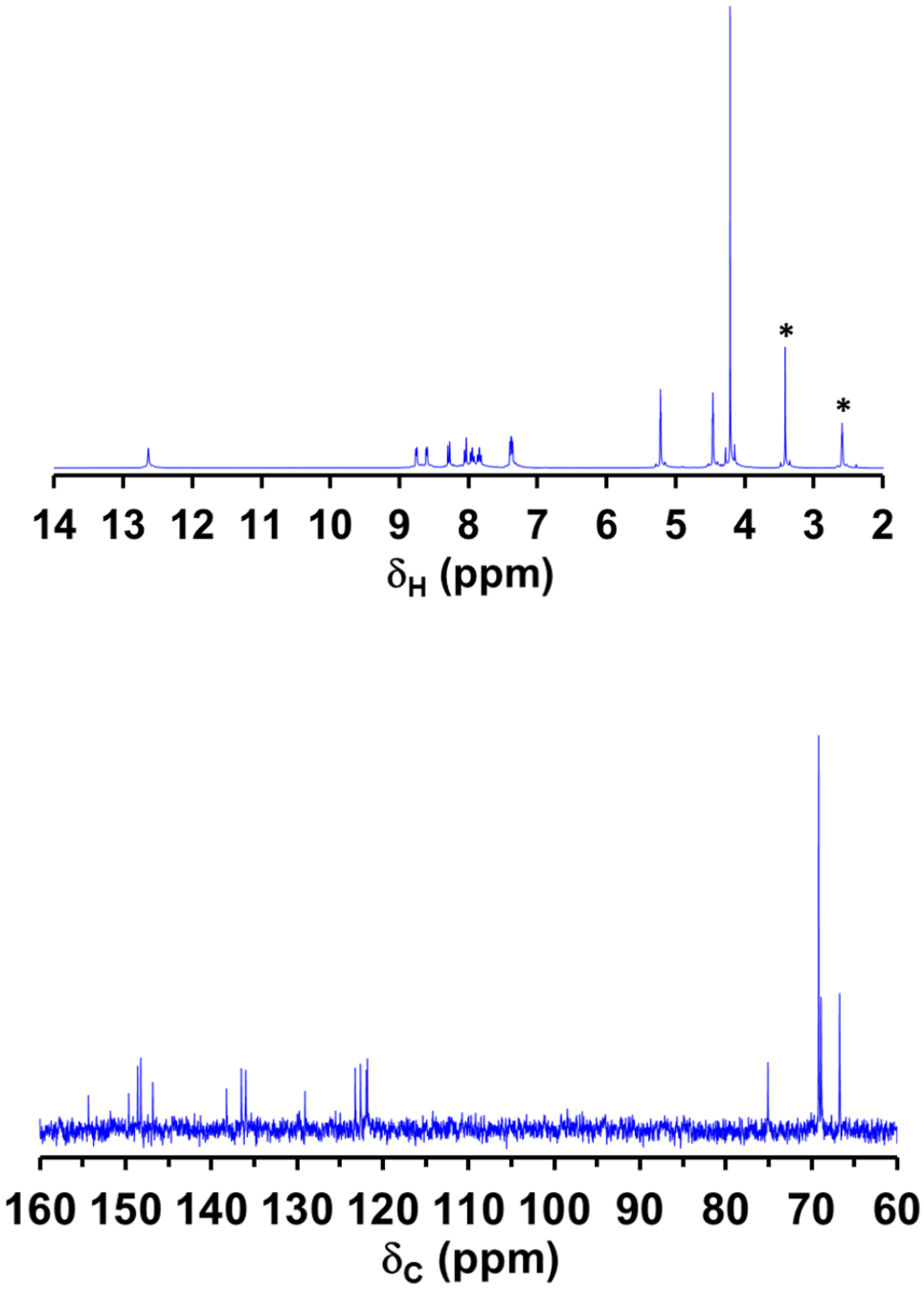

Figure S14. ^{1}H and ^{13}C NMR spectra of **1** in CD_3CN.

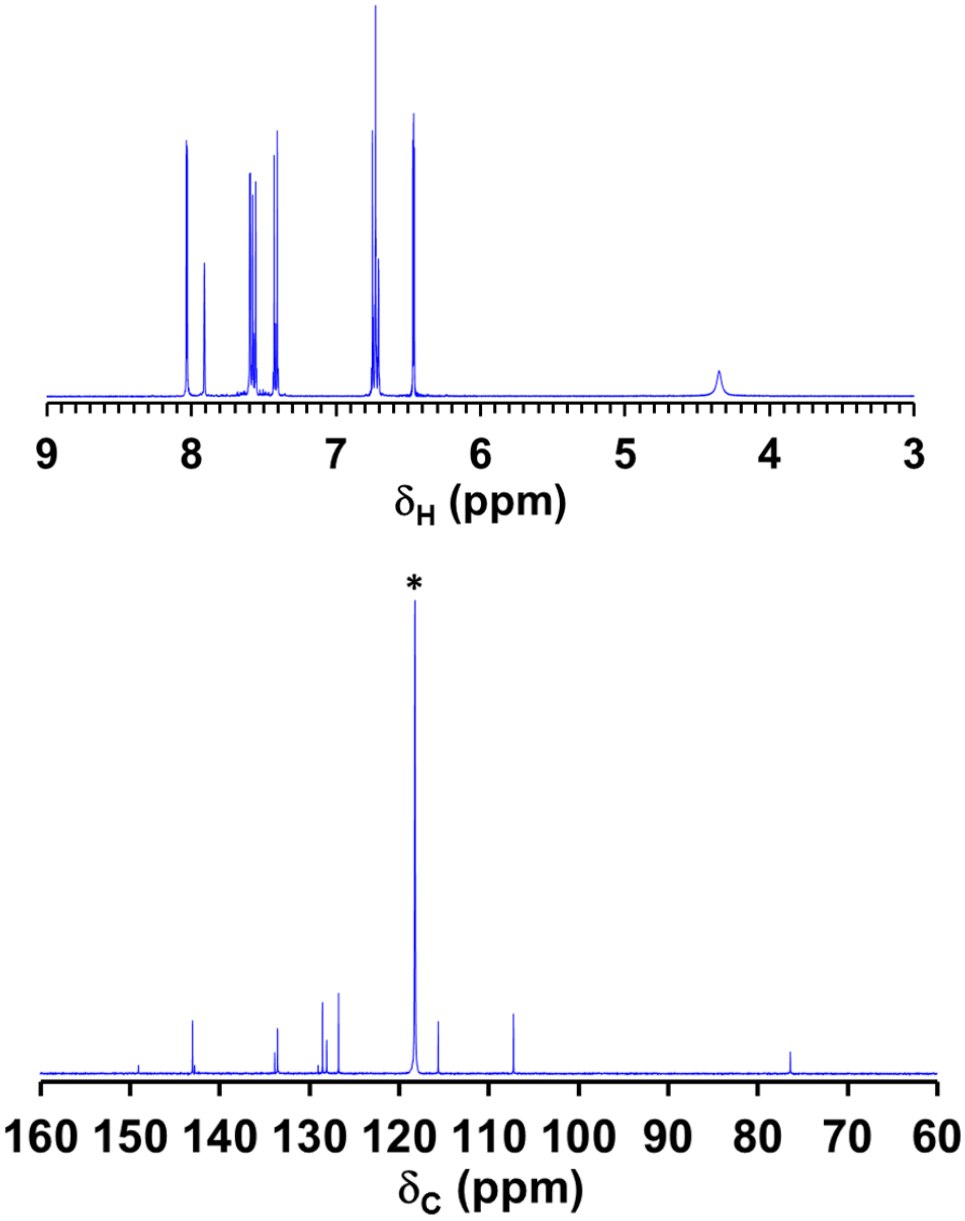

Figure S15. ^{1}H and ^{13}C NMR spectra of **2**·CH_2Cl_2 in dmso-d_6. Asterisks indicate solvent signals while "D" indicates the signal for CH_2Cl_2 solvate molecule.

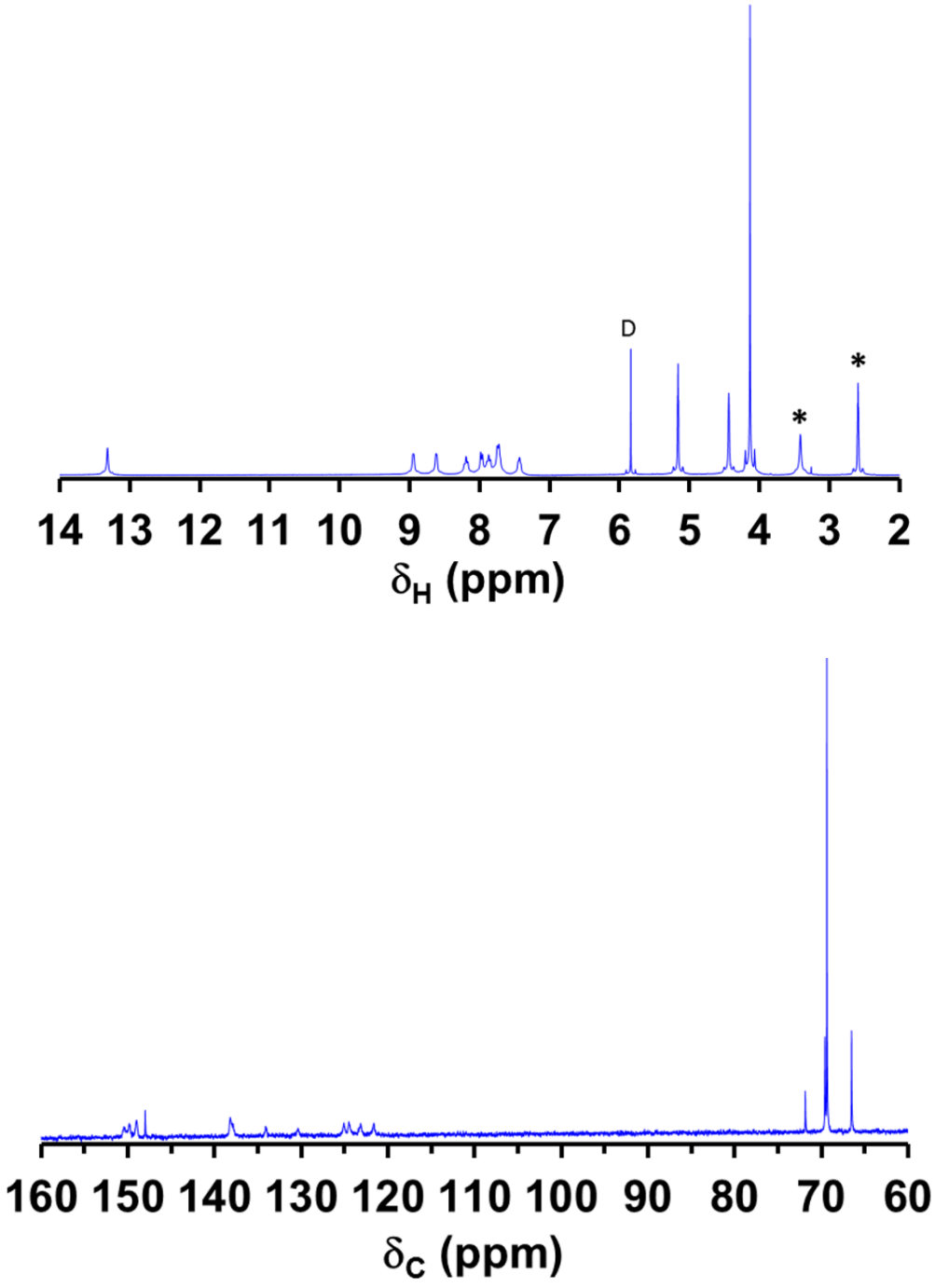

References

[S1] Coulson; D. R.; Satek, L. C.; Grim, S. O. *Inorg. Synth*. **1990**, *28*, 107-109.

[S2] Zapata, F.; Caballero, A.; Espinosa, A.; Tarraga, A; Molina, P. *J. Org. Chem.*, **2008**, *73*, 4034-4044.

[S3] (a) Goreshnik, E.; Mazej, Z. *Solid State Sci.* **2005**, 7, 1225–1229. (b) Greenwood, N.N. *J. Chem. Soc.* **1959**, 3811-3815.

[S4] CrysAlisPro, Agilent Technologies,Version 1.171.34.46 (release 25-11-2010 CrysAlis171 .NET), (compiled Nov 25 2010,17:55:46).

[S5] SAINT+ Version 7.23a and SADABS Version 2004/1. Bruker Analytical Xray Systems, Inc., Madison, Wisconsin, USA, 2005.

[S6] O. V. Dolomanov, L. J. Bourhis, R. J. Gildea, J. A. K. Howard and H. Puschmann. "OLEX2: a complete structure solution, refinement and analysis program". *J. Appl. Cryst.* **2009**, *42*, 339-341.

[S7] Sheldrick, G. M. SHELXTL Version 6.12; Bruker Analytical X-ray Systems, Inc., Madison Wisconsin, USA, 2001.

[S8] F. H. Allen, *Acta Cryst.*, **2002**, *B58*, 380-388.